Astronomy & Astrophysics manuscript no. INT˙fin March 17, 2005
(DOI: will be inserted by hand later)

INTEGRAL observations of SS433: Results of coordinated campaign

A.M. Cherepashchuk[1], R.A. Sunyaev[2,3], S.N. Fabrika[4], K.A. Postnov[1,10], S.V. Molkov[2], E.A. Barsukova[4], E.A. Antokhina[1], T.R. Irsmambetova[1], I.E. Panchenko[1], E.V. Seifina[1], N.I. Shakura[1], A.N. Timokhin[1], I.F. Bikmaev[5], N.A. Sakhibullin[5], Z. Aslan[6,7], I. Khamitov[6], A.G. Pramsky[4], O. Sholukhova[4], Yu.N. Gnedin[8], A.A. Arkharov[8], V.M. Larionov[9]

[1] Sternberg Astronomical Institute, Universitetsky pr. 13, 119992, Moscow, Russia
[2] Space Research Institute, Russian Academy of Sciences, Profsoyuznaya 84/32, 117810 Moscow, Russia
[3] Max-Planck-Institute für Astrophysik, Karl-Schwarzschild-Str. 1, D-85740 Garching bei München, Germany,
[4] Special Astrophysical Observatory, Nizhnij Arkhyz, Karachaevo-Cherkesiya, 369167, Russia
[5] Kazan State University, Kremlevskaya str.18, 420008, Kazan, Russia
[6] TUBITAK National Observatory, Akdeniz Universitesi Yerleskesi, 07058 Antalya, Turkey
[7] Akdeniz University, Physics Department, 07058 Antalya, Turkey
[8] Pulkovo Observatory, St.-Petersburg, Russia
[9] St.-Petersburg University, Russia
[10] University of Oulu, Finland

Abstract. Results of simultaneous *INTEGRAL* and optical observations of galactic microquasar SS433 in May 2003 and *INTEGRAL* /RXTE observations in March 2004 are presented. Persistent precessional variability with a maximum to minimum uneclipsed hard X-ray flux ratio of ~ 4 is discovered. The 18-60 keV X-ray eclipse is found to be in phase with optical and near infrared eclipses. The orbital eclipse observed by *INTEGRAL* in May 2003 is at least two times deeper and apparently wider than in soft X-ray band. The broadband X-ray spectrum 2-100 keV simultaneously detected by RXTE/INTEGRAL in March 2004 can be described by bremsstrahlung emission from optically thin thermal plasma with $kT \sim 30keV$. The optical spectroscopy with the 6-m SAO BTA telescope confirmed the optical companion to be an A5-A7 supergiant. For the first time, spectorscopic indications of a strong heating effect in the optical star atmosphere are found. The measurements of absorption lines which are presumably formed in the non-illuminated side of the supergiant yield its radial velocity semi-amplitude $K_v = 132 \pm 9$ km/s.
The analysis of the observed hard X-ray light curve and the eclipse duration, combined with spectroscopically found optical star radial velocity corrected for the strong heating effect, allows us to model SS433 as a massive X-ray binary. Assuming that the hard X-ray source in SS433 is eclipsed by the donor star that exactly fills its Roche lobe, the masses of the optical and compact components in SS433 are suggested to be $M_v \approx 30 M_\odot$ and $M_x \approx 9 M_\odot$, respectively. This provides further evidence that SS433 is a massive binary system with supercritical accretion onto a black hole.

Key words. stars: individual: SS433 – stars: binaries: eclisping – X-rays: binaries

1. Introduction

SS433 is a massive eclipsing X-ray binary system at advanced evolutionary stage. It is recognized as a supercritically accreting microquasar with precessing accretion disk and mildly relativistic ($v \approx 0.26c$) jets. Since the discovery in 1978 (Clark and Murdin 1978, Margon et al. 1979), this unique X-ray binary has been deeply investigated in optical, radio, and X-rays (see reviews Margon 1984, Cherepashchuk 1988, 2002 and Fabrika 2004 for more detail and references).

Among a dozen of known microquasars SS433 is distinguished by its unique properties.

1). In this system the optical star fills its Roche lobe and mass transfer occurs on thermal time scale with a huge rate of $\dot{M} \sim 10^{-4} M_\odot$ per year and accretion onto the relativistic object is supercritical (Shakura and Sunyaev 1973).

2). Two strongly collimated ($\sim 1^\circ$) oppositely directed jets emanate with a velocity of $80,000 \pm 1,000$ km per

Send offprint requests to: cher@sai.msu.ru

second from the center of the accretion disk. The jets are observed not sporadically, as in most microquasars, but persist over tens of years with virtually constant velocity.

3). The accretion disk and relativistic jets regularly precess with a period of 162.5 days. Both the precession period and the disk inclination angle to the orbital plane ($\sim 20°$) keep on average constant over tens of years.

4). The source exhibits orbital eclipsing periodicity with period $P_{orb} = 13^d.082$. The shape of the optical light curve varies significantly with precessional phase (Goranskij et al. 1998ab, Cherepashchuk and Yarikov 1991). The orbital period is found to be very stable over more than 25 years, despite the intensive mass exchange rate between the binary components and strong wind mass loss ($v \approx 2000$ km/s, $\dot{M} \simeq 10^{-4} M_\odot$/yr) from the supercritical accretion disk.

The unsolved puzzles of SS433 still remain to be solved include: (1) the nature of the relativistic object, (2) the mechanism of collimation and acceleration of matter in jets to the relativistic velocity $\sim 80,000$ km/s, (3) the nature of the precessional phenomena in this X-ray binary system (Chakrabarti, 2002).

The *INTEGRAL* observations of SS433 in 2003 discovered hard (up to 100 keV) X-ray spectrum in this supercritically accreting microquasar (Cherepashchuk et al. 2003, 2004), suggesting the presence of an extended hot (with a temperature up to 10^8 K) region at the central parts of the accretion disk. These new data made it possible to compare the eclipse characteristics of SS433 at different energies: soft X-rays (2-10 keV, the *ASCA* data), soft and medium X-ray (1-27 keV, the *Ginga* data), hard X-rays (20-70 keV, the *INTEGRAL* data), and the optical. This comparison allows us to investigate the innermost structure of the supercritical accretion disk and to constrain the basic parameters of the binary system .

This paper is organized as follows: Section 2 lists the participants of the observational campaign. Section 3 describes the obtained X-ray spectra and light curves. Section 4 presents the analysis of hard X-ray precessional and orbital variability of SS433. Section 5 reports the results of optical and infrared photometry. Section 6 describes in detail the simultaneous optical spectroscopy of SS433 obtained with the 6-m BTA telescope and the measurements of the optical radial velocity curve. Implications of our observations to binary masses in SS433 are summarized in Section 7, and Sections 8 and 9 contain the discussion and conclusions, respectively.

2. Observational campaign

The coordinated multiwavelength observational campaign of SS433 was organized during the *INTEGRAL* observations of the SS433 field in March-June 2003 with the participation of the following research teams.

1. Special Astrophysical Observatory of Russian Academy of Science (SAO RAS). High signal-to-noise optical spectroscopy of SS433 at the 6-m telescope was performed.

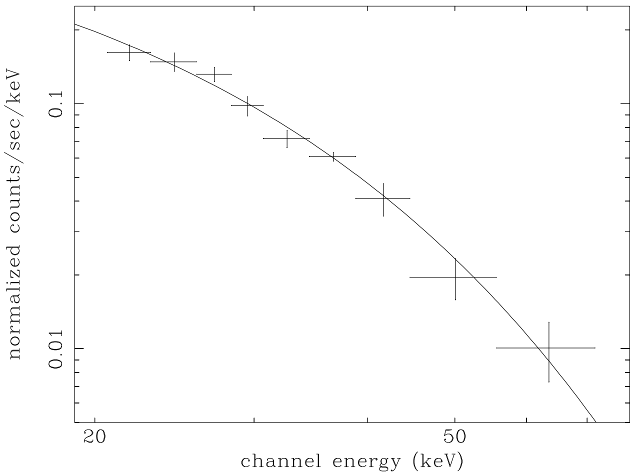

Fig. 1. IBIS/ISGRI spectrum of SS433 collected over *INTEGRAL* orbits 67-69 in May 2003. The best fit (solid line) is for exponential cut-off with $E_c = 14 \pm 2$ keV. Reduced $\chi^2 = 0.32$ for 7 degrees of freedom (dof), $CL \approx$ 95%.

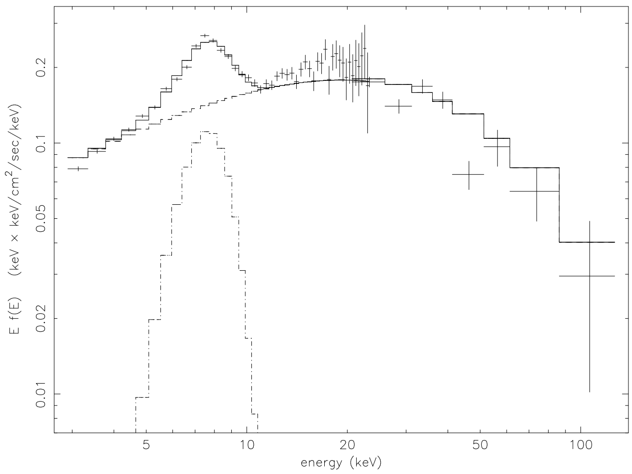

Fig. 2. RXTE PCA and IBIS/ISGRI spectrum of SS433 obtained during simultaneous *RXTE/INTEGRAL* observations of SS433 in March 24-27, 2004. The best fit (solid line) is for bremsstrahlung emission from optically thin plasma with $kT = 29.0 \pm 0.7 keV$ (model "bremss" from the XSPEC package). Reduced $\chi^2 = 0.77$ for 50 dof, $CL \approx 88\%$.

2. Crimean Station of Sternberg Astronomical Institute. BVR-photometry at the 0.6-m telescope was obtained.

3. Kazan State University. The optical photometry at the Russian-Turkish 1.5-m telescope RTT-150 at the TUBITAK National Observatory (Turkey) was carried out.

4. Infrared K-photometry was performed at 1.1-m AZT-24 telescope of Pulkovo Observatory in Italy, Osservatorio di Campo Imperatore.

5. Radio monitoring at cm wavelength has been performed at the RATAN-600 radio telescope of SAO RAS.

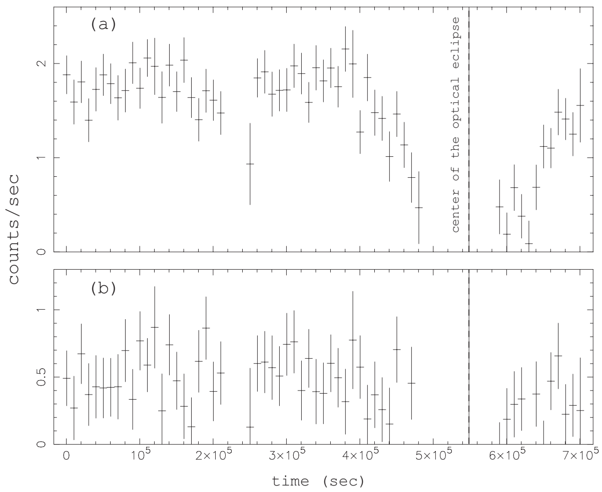

Fig. 3. IBIS/ISGRI 20-40 keV (upper panel) and 40-70 keV (bottom panel) count rates of SS433 (without background subtraction) obtained in May 2003. Origin of time is MJD= 52763.95. The egress part of the X-ray eclipse was kindly provided by Dr. Diana Hannikainen.

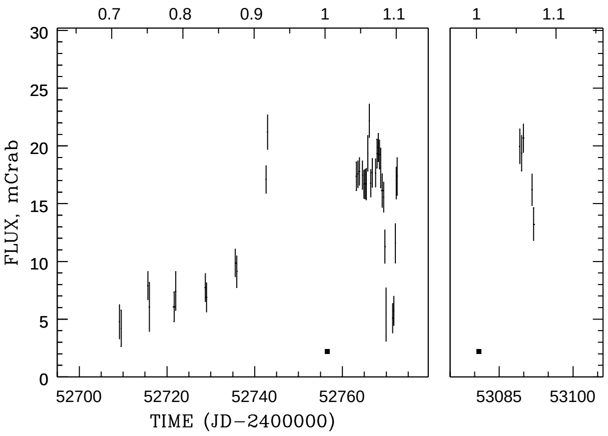

Fig. 4. Precessional hard X-ray (25-50 keV) variability of SS433. Left panel: March-May 2003. Right panel: March 2004. The filled squares mark the T3 precession phase according to ephemeris by Goranskij et al. **[1998ab]**. The upper axis shows the precessional phase according to the same ephemeris.

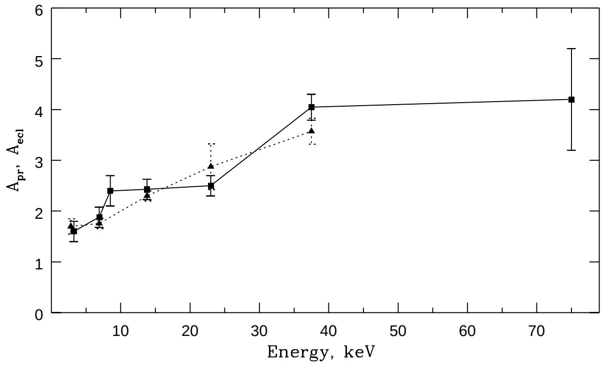

Fig. 5. The precession and eclipse amplitudes of SS433 at different energies in the quiet state: A_{pr} (squares and solid line) and A_{ecl} (triangles and dashed line).

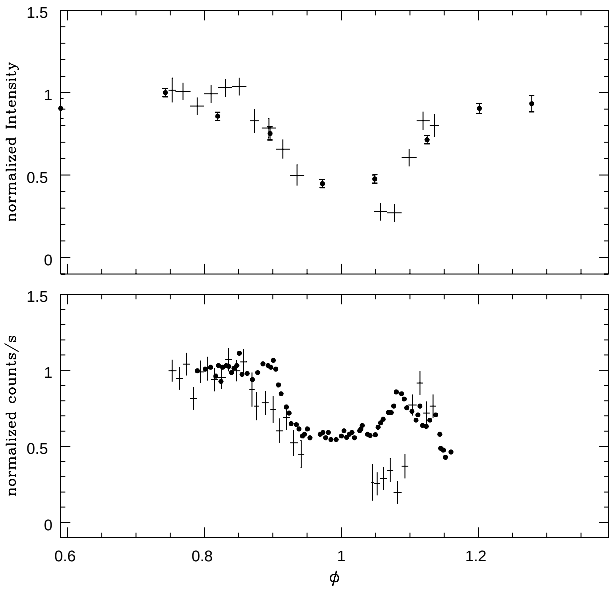

Fig. 6. The primary X-ray eclipse of SS433 in the 18-60 keV energy band. IBIS/ISGRI data (May 2003). Upper panel: X-ray light curve averaged over 20000 s (10 *INTEGRAL* science windows, SCW) superimposed on the simultaneously obtained V optical photometric light curve (Crimea, SAO). Bottom panel: the same hard X-ray eclipse light curve averaged over 10000 s (5 SCW) superimposed on the *Ginga* 4.6-27 keV eclipse (filled circles; from Kawai et al. 1989, Yuan et al. 1995) taken at about the same precession phase. The *INTEGRAL* data is the same on both panels, but the averaging is different.

The source was found to be at its non-flaring (quiet) state in May 2003 (Trushkin 2003).

SS433 was within the field of view of the IBIS telescope during the *INTEGRAL* observations (March 2004) of the Sagittarius arm tangent region centered to $l = +40°, b = 0°$. We included part of these observations in our analysis. In contrast to the observations in May 2003, radio monitoring showed that SS433 had been in its flaring (active) state (Trushkin 2004).

3. IBIS/ISGRI light curves and spectra

The *INTEGRAL* IBIS/ISGRI data were analyzed using both publicly available ISDC software (OSA-3 version) and the original software elaborated by the IKI *INTEGRAL* team (see Revnivtsev et al. 2004b for more detail). The latter allows better sensitivity in constructing maps and spectra to be achieved. The main results can be summarized as follows.

Table 1. Best-fit parameters of the joint RXTE+*INTEGRAL* spectrum of SS433 observed in March 24-27, 2004. The model is bremsstrahlung emission and a gaussian emission line (from the XSPEC package). The energy of the emission line was a free parameter. The physical nature of the line is not discussed in the present paper.

Parameter	kT (kev)	Gaussian emission line energy (keV)	Gaussian sigma (keV)
Value	28.9 ± 0.7	7.26 ± 0.03	1.2 ± 0.04

A. The IBIS/ISGRI spectrum of SS433 (25-100 keV) in May 2003 as processed by the OSA-3 software can be fitted by a power-law $\sim E^{-\alpha}$ with photon index $\alpha \approx 2.7 \pm 0.13$, taking into account the 10% systematic errors. **A satisfactory fit is obtained also with exponential cut-off** $\exp(-E/E_c)$ with $E_c \sim 12-16$ keV (Fig. 1).

The integrated hard X-ray luminosity in May 2003 was $L_x(18-60\mathrm{keV}) \sim 4 \times 10^{35}$ erg/s, $L_x(60-120\mathrm{keV}) \sim 2 \times 10^{35}$ erg/s (assuming the 5 kpc distance to SS433), which is about 10% of the soft X-ray jet luminosity.

Using the OSA-3 software, we could not detect significantly the source in the JEM-X data. Instead, we made use of more detailed *RXTE* observations of SS433 performed simultaneously with *INTEGRAL* in March 2004 to obtain the broadband 2-100 keV spectrum of SS433. The source was observed a few days after the disk maximum opening phase. The OSA-3 software also did not allow us to detect significantly the source at energies above 70 keV, so we used the IKI software to obtain the SS433 spectrum up to 100 keV. This software has proven its quality and efficiency in processing *INTEGRAL* observations of the Galactic center (Revnivtsev et al. 2004b).

The resulting broadband X-ray spectrum of SS433 in March 2004 is shown in Fig. 2. It can be adequately fitted by the bremsstrahlung emission from optically thin thermal plasma with $kT \sim 30$ keV (model "bremss" from XSPEC package was used; see Table 1). The reduced chi-square value for 50 dof is ~ 0.8, which corresponds to a null hypothesis probability of ~ 0.9.

B. The IBIS/ISGRI count rates of SS433 in May 2003 are presented in Fig. 3. The X-ray eclipse at hard energies is observed to be a little narrower than the optical one, slightly broader than in the 4.6-27 keV *Ginga* energy range and displays extended wings (Fig. 6). This is opposite to what is found in ordinary eclipsing X-ray binaries (like Cen X-3, Vela X-1 etc.), in which the X-ray eclipse duration decreases with energy.

C. The eclipse depth is observed to be at least 80% in hard X-rays compared to $\sim 50\%$ in 4.6-27 keV band (Fig. 4-6).

D. The 25-50 keV X-ray flux increases from ~ 5 to ~ 20 mCrab during March-May 2003 when the source precessed from the crossover (T2) phase to the maximum opening disk phase (T3). This modulation is ~ 2 times larger than observed in the 2-10 keV energy band (see Fig. 5). Thus,

Table 2. Change of the precession amplitude of SS433 A_{pr} with energy

Energy range keV	A_{pr}	Data	Ref.
1.5-5	1.6	ASM/RXTE	[1]
4.6-9.2	1.88	*Ginga*	[2,3]
5-12	2.4	ASM/RXTE	[1]
9.2-18.4	2.43	*Ginga*	[2,3]
18.4-27.6	2.5	*Ginga*	[2,3]
25-50	4	*INTEGRAL*	[4]
50-100	4.2	*INTEGRAL*	[4]

[1] - Fabrika et al. 2004; [2] - Kawai et al. 1989; [3] - Yuan et al. 1995; [4] - Cherepashchuk et al. 2003

both precessional and eclipsing hard X-ray variabilities in SS433 exceed by ~ 2 times those in the standard X-ray band (Fig. 5). This suggests a more compact vertical structure of hard X-ray emitting region in the central parts of the accretion disk.

4. Analysis of precessional and orbital variability of SS433 in the 25-50 keV energy range

4.1. Precession variability

As mentioned above, the 25-50 keV flux of SS433 varies from $F_{min} \sim 5$ mCrab to $F_{max} \sim 20$ mCrab, with F_{min} and F_{max} corresponding to precession phases of the disk seen edge-on (moment T2) and maximum open (moment T3), respectively, yielding the ratio $A_{pr} \equiv F_{max}/F_{min} \sim 4$. In Fig. 4 we present all available for us *INTEGRAL* observations of SS433. The left panel shows the 2003 data (*INTEGRAL* orbits 49, 51, 53, 56, 58, 60, 67-70). The right panel shows the 2004 data (March 24-25, orbits 176 and 177). It is seen that the uneclipsed flux of SS433 in 2004 (we remind that the source was observed near the T3 phase) is comparable within the errors with the maximum flux observed near the T3 phase in 2003 (these phases are indicated by the filled squares). This suggests that the precessional hard X-ray variability of SS433 keeps constant at least over several precessional cycles.

The amplitude of the precession variability in SS433 in different X-ray bands appears to be monotonically increasing with energy (Fig. 5, the squares and the solid line; Table 2). For example, archive RXTE/ASM data collected over several years (only quiet states of SS433 have been selected) indicate that $A_{pr}(1.5-5\mathrm{keV}) = 1.6$, $A_{pr}(5-12\mathrm{keV}) = 2.4$ (Fabrika et al. 2004). The errors are due to the SS433 flux at the crossover being heavily absorbed (especially at the first crossover). The *Ginga* data (Kawai et al. 1989, Yuan et al. 1995) also fit this dependence (Table 2). The monotonic increase of the precession amplitude with energy is consistent with the model of emitting region in SS433 as a cooling outflow.

For a jet of finite length or consisting of individual evolving fragments with finite life times (Lind and Blandford 1985; Begelman et al. 1984; Panferov and

Table 3. Primary X-ray eclipse depth A_{ecl} variations with energy

Energy keV	$\langle E \rangle$ keV	A_{ecl}	Data	Ref.
1.0-4.6	2.8	1.7	*Ginga*	[1,2]
4.6-9.2	6.9	1.8	*Ginga*	[1,2]
9.2-18.4	13.8	2.3	*Ginga*	[1,2]
18.4-27.6	23.0	2.9	*Ginga*	[1,2]
25-50	37.5	3.6	*INTEGRAL*	[3]

[1] - Kawai et al. 1989; [2] - Yuan et al. 1995; [3] - Cherepashchuk et al. 2003

Fabrika 1997), the intensity of radiation in the jet rest frame is $\mathcal{J}_{co} = (1+z)^{2+\alpha}\mathcal{J}_{obs}$, where $\mathcal{J}_{obs}$ is the observed intensity of the jet emission, $z = -\delta\nu/\nu$ is negative for the approaching jet and α is the spectral index ($I_\nu \propto \nu^{-\alpha}$). With appropriate values of the spectral index, the precession amplitude due to the relativistic beaming only in the case where both jets are always seen and are not screened by the accretion disk would be ~ 1.1, and in the case that the receding jet is fully screened by the disk it would be ~ 1.5. So the large (~ 4 times) precession variability found in the hard X-ray band 25-50 keV can not be explained by the jet relativistic beaming only and should be almost fully caused by geometric screening of the inner disk structure producing hard X-rays by the edge of the precessing thick accretion disk. The precession light curve in the 25-50 keV energy band exhibits a significant irregular variability which is apparently related with nonstationarity of the outer edges of a geometrically thick accretion disk.

4.2. Hard X-ray eclipse

The *INTEGRAL* observations in May 9-11, 2003, enable us to study in detail its hard X-ray eclipse. We have used our data on May 9 and 11. Data on May 10, 2003 were kindly given us by Dr. Diana Hannikainen. The main eclipse falls to the precession phase $\psi_{pr} = 0.09$ (according to ephemeris by Goranskij et al. 1998a), fairly close to the T3 (disk maximum opening) phase.

The primary X-ray eclipse in the 18-60 keV energy band (IBIS/ISGRI data) is plotted in Fig. 6. The points are averaged over 5 and 10 *INTEGRAL* scientific windows (10000 and 20000 s, respectively). For comparison, we plot 4.6-27 keV X-ray eclipse observed by *Ginga* (Kawai et al. 1989, Yuan et al. 1995) at about the same precession phase. The upper panel in Fig. 6 also shows optical (V) light curve observed simultaneously with *INTEGRAL* in Crimea and SAO (see below). The upper panel is shown here to demonstrate the absence of any noticeable lag between optical and hard X-ray primary eclipses.

The inspection of Fig. 6 reveals that the *INTEGRAL* eclipse is **up to two times deeper than** that observed by *Ginga* at softer X-ray band. The ascending branch of the hard 18-60 keV eclipse clearly shows some irregularities. These features are similar to those observed by *Ginga* in the softer 4.6-27 keV X-ray band. If this is indeed the case, we can take the upper envelope of the ascending branch of the X-ray eclipse light curve as a representative shape of the eclipse by the optical star body. Note that the X-ray eclipse minimum observed by *Ginga* was consistent with the synchronously observed optical one (Aslanov et al. 1993). This proves that there is no appreciable phase shift between the middle of the *INTEGRAL* and *Ginga* X-ray eclipses shown in Fig. 6.

The X-ray eclipse depth as a function of energy is shown in Fig. 5 by the dotted line. The eclipse depth A_{ecl} was defined as the ratio of the mean uneclipsed flux before the eclipse to the middle eclipse flux at the T3 precession phase of SS433 in the quiet state. These data are collected in Table 3. Note the tendency for A_{ecl} to increase with energy, which may mean that the hotter parts of the X-ray emitting region located closer to its base are totally eclipsed by the optical star.

The dependence of the precession amplitude and X-ray eclipse depth on energy is the same, suggesting similar screening efficiency of the X-ray emitting region by the accretion disk edge and by the optical star. This means that the size of the accretion disk can be comparable with that of the optical star. Such a conclusion has been also inferred from optical photometry (Fabrika & Irsmambetova 2002; Fabrika 2004).

4.3. The geometric model of the system

To interpret the X-ray light curve of SS433 we used a geometric model applied earlier to the analysis of the *Ginga* X-ray eclipse (Antokhina et al. 1992). We consider a close binary system consisting of an opaque "normal" star limited by the Roche equipotential surface and a relativistic object surrounded by an optically and geometrically thick "accretion disk". The "accretion disk" includes the disk itself and an extended photosphere formed by the outflowing wind. The orbit is circular, the axial rotation of the normal star is synchronized with the orbital revolution.

The disk is inclined with respect to the orbital plane by an angle θ. The opaque disk body (see Fig. 7) is described by the radius r_d and the opening angle ω. The central object is surrounded by a **transparent** homogeniously emitting spheroid with a visible radius r_j and height b_j, which could be interpreted as a "corona" or a "jet" (without any relativistic motions).

Here r_j, b_j and r_d are dimensionless values expressed in units of the binary separation a. The radius of the normal (donor) star is determined by the relative Roche lobe size, i.e. by the mass ratio $q = M_x/M_v$ (M_x here denotes the mass of the relativistic object).

Only the "corona" is assumed to emit in the hard X-ray band, while the star and disk eclipse it in due course of the orbital and precessional motion. During precession the inclination of the disk with respect to the observer changes, causing different conditions of the "corona" visibility. So observations of the precessional variability can be

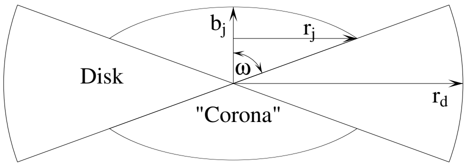

Fig. 7. Geometrical model of the accretion disk and its "corona".

used to obtain a "vertical" scan of the emitting structure, restricting the parameters b_j and ω. The orbital (eclipse) variability observations scan the the emitting structure "horizontally" , restricting possible values of r_d, ω, q and r_j. The joint analysis of precessional and eclipse variability enables us to reconstruct the spatial structure of the region in the accretion disk center where the hard X-rays are produced.

The position of the components of the system relative to the observer is determined by the binary orbit inclination angle $i = 78.8°$, the disk inclination angle to the orbital plane $\theta = 20.3°$, the precession phase ψ_{pr} with $\psi_{pr} = 0$ at the maximum disk opening of SS433 (T3, maximum separation between the moving emission lines) and $\psi_{pr} = 0.34, 0.66$ when the disk is seen edge-on (at the moving emission line crossover moments T1 and T2, respectively).

To analyze the X-ray eclipse and precession light curve observed by *INTEGRAL* we have used the following three model shapes of the hard X-ray emitting region which can be parametrized by two parameters r_j and b_j: long narrow jets($r_j \ll b_j \sim a$), short narrow jets ($r_j \ll b_j \ll a$), and short thick "jets", or corona ($r_j > b_j$). For all models the formal χ^2 minimum is reached for a maximum allowed accretion disk radius r_d and the disk opening angle $\omega \sim 90°$ (see discussion below). **The accretion disk radius was limited by the distance from the relativistic object center to the inner Lagrangian point, which exceeds the radius of the Roche lobe around the compact star. This is natural for a supercritical accretion disk with a strong radial outflow (Zwitter, Calvani & D'Odorico, 1991). Further extension of the accretion disk is not justified because of the presence of narrow absorption lines of the optical A5-A7 component in the spectrum, which means that there is no appreciable screening of the oprical star by the disk. Such an extension of the disk would mean that the binary system is on the common envelope evolutionary stage, and so the narrow absorption lines from the optical star surface could not be observed. The orbital period stability during 30 years of observations also evidences against the presence of a common envelope in SS 433.**

The results of our analysis can be summarized as follows.

1. Long narrow jets ($r_j \ll b_j \sim a$) outflowing from the central object can be only partially screened by the disk during its eclipse and precession. Neither the observed eclipse depth nor the precession amplitude $A_{pr} \sim 4$ can be explained by this model. (See Fig. 8).

2. Short narrow jets ($r_j < b_j \ll a$) where b_j is found from the condition that the precession variability amplitude is $A_{pr} = 4$. The theoretical eclipse light curves for this model for different mass ratios q are displayed in Fig. 9. For any q this model is inconsistent with the observed 18-60 keV X-ray eclipse shape.

3. Extended corona ($r_j > b_j$) gives the best fit for the observed hard X-ray precession amplitude ($A_{pr} \sim 4$) and the observed eclipse shape (Fig. 10). Minimum residuals in this model are attained for the mass ratio $q = m_x/m_v \approx 0.2$ (Fig. 11), which is close to that derived from fitting the *Ginga* and *ASCA* observations with a narrow jet model (Kawai et al. 1989, Kotani et al. 1996). If we take into account only the upper envelope of the ascending X-ray eclipse branch (see above), **the fit with $q \approx 0.3$ seems to be acceptable to be as well** (Fig. 10 and 11).

The parameters b_j and ω appear to be related and cannot be determined separately. Formal χ^2 decreases as

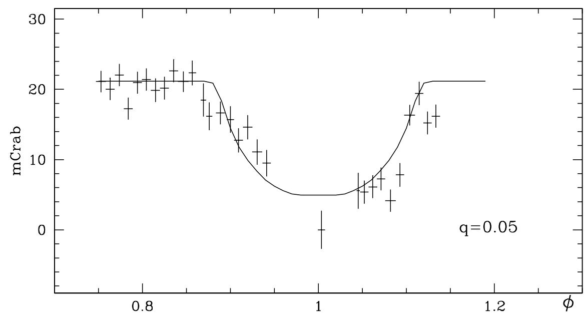

Fig. 8. X-ray eclipse fit with a model of narrow long X-ray emitting jets. Precession variability cannot be reproduced by this model though the eclipse shape is fitted. The point at the center of eclipse was taken from the Galactic Plane Survey scan in the beginning of the 70th *INTEGRAL* orbit

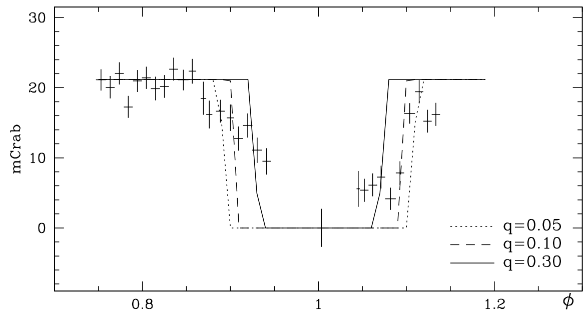

Fig. 9. The same as in Fig.8 but for a model of narrow short X-ray emitting jets for different values of q. Precession variability amplitude $A_{pr} = 4$ is reproduced, but the eclipse shape is not.

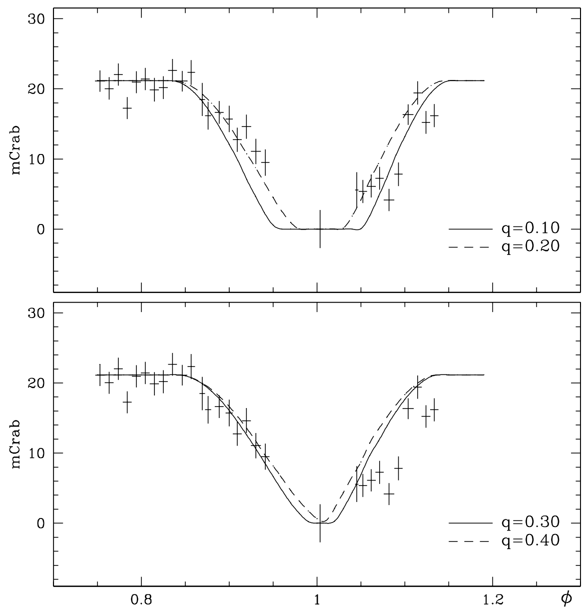

Fig. 10. The same as in Fig. 8 but with a model of the extended oblate X-ray emitting region ("corona") for different q. The precession variability amplitude is $A_{pr} = 4$.

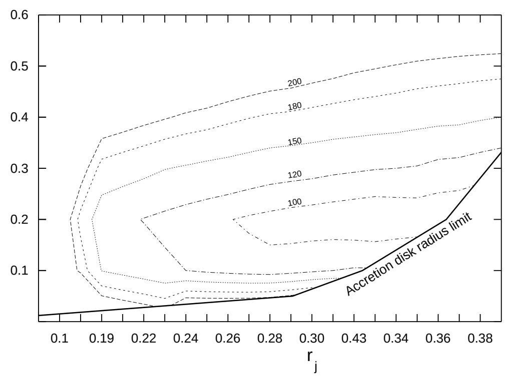

Fig. 11. χ^2 map (26 dof) in the plane (r_j, q) **for models with an extended oblate X-ray emitting region. The outer edge of the accretion disk limited by the distance to the inner Lagrangian point is shown by the solid line.** The precession variability amplitude is $A_{pr} = 4$.

$\omega \to 90°$, without any essential change of q for $\omega \gtrsim 80°$. Obviously, the solution with $\omega = 90°$ (planar disk with zero thickness) could not provide any precessional variability, so we accepted $\omega \sim 80°$. This also agrees with the estimates of the thickness of accretion disk from the rapid optical and X-ray variability corellation (Revnivtsev et al., 2004a).

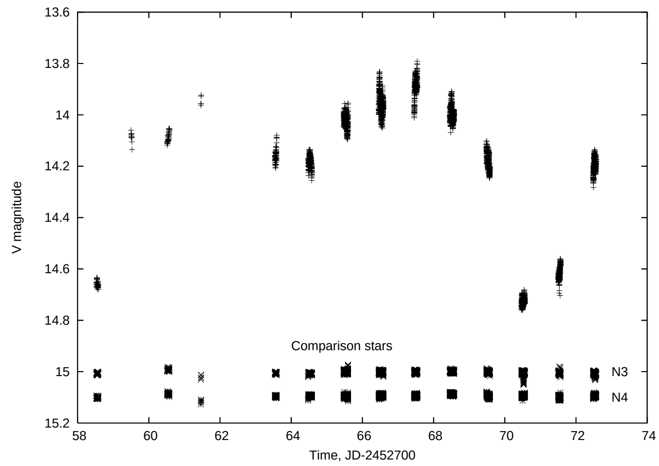

Fig. 12. V-light curve of SS 433 obtained at the RTT150 telescope (TUBITAK National Observatory, Turkey) simultaneously with *INTEGRAL* observations. In the bottom: photometry of control stars ($V_{N3} = 12.93, V_{N4} = 12.70$).

From this analysis we conclude that in the frame of our geometrical model the hard X-ray emitting region in SS433 the observed precession amplitude and X-ray eclipse shape are best reproduced by a broad oblate corona above an optically thick accretion disk. The best fit parameters are $r_j \sim 0.3$, $b_j \sim 0.1$ and $\omega \sim 80°$, the mass ratio $q = 0.2 - 0.3$.

Physically, such a corona could be thought of as hot rarefied plasma filling the funnel around the jets. In this picture outer parts of long thin jets that are not screened by the funnel walls are responsible for emission in soft X-rays, while the more extended hot corona inside the funnel produces hard X-ray flux. The estimation of the funnel size $\sim 10^{12}$ cm was obtained by Revnivtsev et al. (2004a) from the analysis of rapid non-coherent variability in SS433. The opening angle of the funnel can be quite large, so the apparent size of the outer funnel which we model here as an extended oblate corona over opaque disk can be comparable with the accretion disk size, as our best fit parameters suggest. **The nature of such a plasma inside the funnel and how it maintains its stationarity requires further studies.** We also note that actual detection accuracy of the hard part of the broadband X-ray spectrum of SS433 obtained by INTEGRAL (Fig. 2) is insufficient to definitely rule out the presence of the two-component structure of X-ray emitting region inferred from our analysis.

5. Optical and IR photometry

5.1. Optical photometry

Photometry of SS433 was performed simultaneously with *INTEGRAL* observations by the Russian-Turkish RTT-150 telescope of Kazan University at the TUBITAK National Observatory, Turkey. **Observations were**

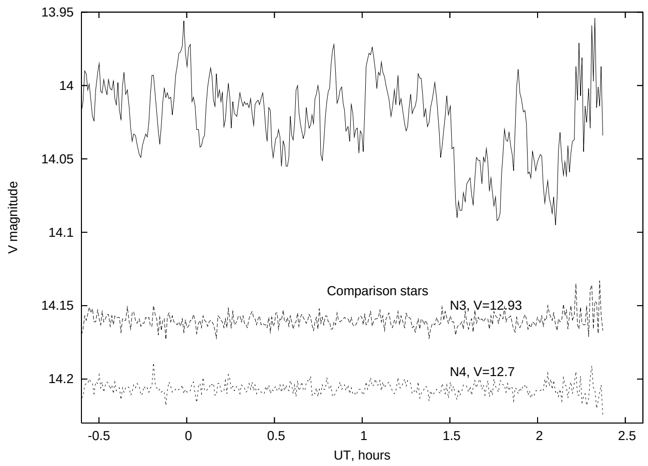

Fig. 13. Rapid photometric variability of SS433 during the night 05/06 May 2003

made by using commercial ANDOR company camera (model DW436, www.andor-tech.com) which is termoelectrically cooled to $-60°$ C. The CCD was provided for RTT150 by MPA. It is a low noise back illuminated model from EEV with 2048 x 2048 pixels of 13.5 μ size. Full field of view is 8 x 8 arcmin with frame reading time of 40 sec at 2 x 2 binning. To increase the time resolution only parts of the field of view with reference stars N 1,2,3,4,5 (Leibowits and Mendelson, 1982) around SS433 were stored to PC. The obtained V-light curve is presented in Fig. 12. Strong ($\sim$ 0.15 mag) intranight variability of the source on timescales $\sim$ 100 s - 100 min is clearly detected (see Fig. 13 for the night 05/06 May 2003).

The mean V light curve during the eclipse obtained at the Crimean Laboratory of SAI (Nauchnyi, Crimea) simultaneously with the *INTEGRAL* **observations was already shown in the upper panel** of Fig. 6. The detector was a pulse-counting, single-channel broad-band WBVR photoelectric photometer installed on the Zeiss-600 reflector. The photometer and software were designed and manufactured by I.I.Antokhin and V.G.Kornilov (SAI). The data were collected in the standard way using differential techniques. The main comparison star was C1 with magnitude $V = 11.51$ (Gladyshev et al. 1980). The typical rms measurement errors in V were 0.02-0.03. The mean V light curve during the *INTEGRAL* observations corresponds to a quiet state of SS433. The optical eclipse minimum is observed at $JD = 2452770.863$, as predicted by the orbital ephemeris given by Goranskij et al. 1998ab.

5.2. IR-photometry

Near IR observations of SS 433 were obtained at AZT-24 1.1m telescope in Campo Imperatore (Italy) during a period spanning July-August 2003. Some observational data were obtained also in October - November 2003. The AZT-24 telescope at the Campo Imperatore Observatory located 2150 m above sea level (a cooperation among Rome, Teramo and Pulkovo Observatories) is basically used for photometric studies of variable sources at near infrared (NIR) wavelengths. The telescope is equipped with a SWIRCAM NIR 256x256 pixels imaging camera which was mounted at the focal plane of AZT-24. This camera was built at the Infrared Laboratories in Tucson (Arizona, USA) and was delivered in 1997 to the laboratories of the Astronomical Observatory of Rome in Monte Porzio. The SWIRCAM is equipped with a PICNIC array, an upgrade of the NIGMOS detector, with a working range of 0.9 - 2.5 μ. It yelds a scale of 1.04 arcsec per pixel resulting in a field of view of 4x4 sq. arcmin. The observations were performed through standard Johnson JHK broadband filters. The NIR monitoring of SS433 started several orbits after the *INTEGRAL* observations. The JHK light curves are presented in Fig. 14. The observations were done close to the crossover precession phase, where the orbital modulation appears to be significantly reduced. Coincidence of the minima in the IR and optical light curves support our general geometrical model.

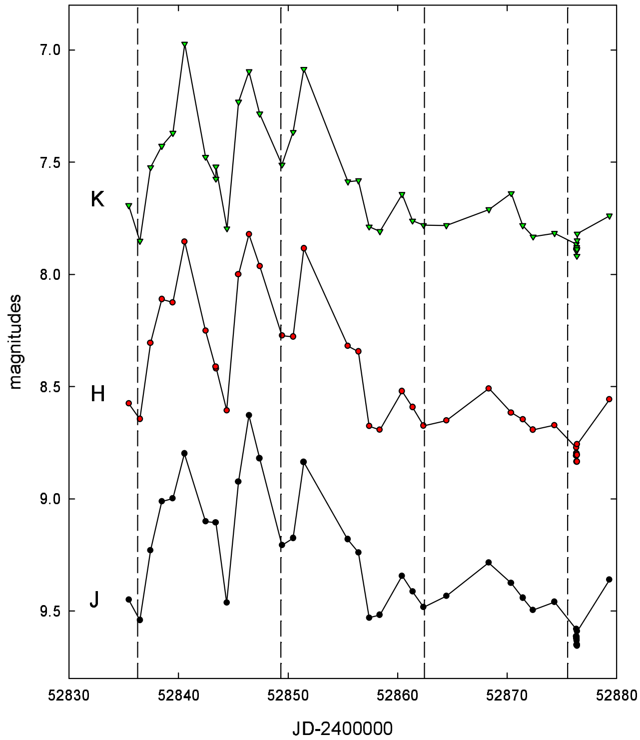

Fig. 14. JHK-photometrical light curve of SS433 obtained by AZT-24 1.1-m IR telescope in July-August 2003 (Campo Imperatore, Italy). The dashed vertical lines mark the primary eclipse of SS433 according to ephemeris by Goranskii et al. (1998a).

6. Optical spectroscopy

6.1. Spectral observations

The optical spectroscopy of SS433 was performed at the 6-m telescope of the Special Astrophysical Observatory during 6 nights on April 28 and May 9-13 2003 simultaneously with the *INTEGRAL* observations at the precessional phase corresponding to the maximum disk opening angle (T3). The Long-Slit spectrograph (Afanasiev et al. 1995) at the telescope prime focus equipped with 1000x1000 Photometrics CCD-detector was used to obtain spectra with a resolution of 3 A (1.2 A/pix). A standard technique was used for spectral reduction and calibration.

Table 4 lists a journal of spectral observations and includes date, JD of the middle of observation, orbital and precessional phases, number of spectra during the night and the mean exposure, and spectral range used. We have taken spectra in the blue region as they are the most informative for searching for the donor star absorption lines (Gies et al., 2002) and include the He II $\lambda4686$ emission line. In two nights we obtained spectra in red region to find orientation of relativistic jets and identify the moving lines in all our spectra. The blue spectral range was shifted redward in the May 2003 observations because of the Moon rising. The signal-to-noise ratio in our spectra averaged over night at $\lambda = 4250$ Åis ≈ 60 per resolution element in May 10-13 and it is ≈ 80 in other dates. The signal-to-noise ratio increases towards longer wavelengths.

6.2. Search for optical star lines

The strongest lines in SS433 — hydrogen, HeI, HeII and some FeII lines appear in emission. Emission line widths in SS433 have FWHM$\sim$ 1000 km/s, corresponding to ~ 10 Å in the blue region. The emission lines are formed in the accretion disk wind and in gas streams in the binary system. A detailed description of the SS433 spectrum may be found in Fabrika (2004). In precession phases close to the crossovers (T2), hydrogen (Hβ and upper lines), HeI and FeII lines have narrow blueshifted absorption components, P Cyg or shell-like profiles, which are formed in gas outflow from the accretion disk. Weaker FeII lines — appear as pure absorptions in these precession phases. The absorption components are also strengthened in orbital phase $\phi \approx 0.1$, they are probably formed in the disk wind interacting with the star (Fabrika et al. 1997).

The absorption components of the shell-like line profiles and even the pure absorption lines should be formed in the disk wind too, which follows from the strong dependences of their intensities (Crampton & Hutchins, 1981) and radial velocities (Fabrika et al. 1997) on the precession phase. Therefore, a search for the donor star spectrum in SS433 should be made with a certain caution. The search should be made among the weakest (photospheric) lines and in precession phases where the extended disk and its outflowing wind do not intersect the line of sight. In addition, stellar lines should to be stronger in the middle of the accretion disk eclipse and weakener outside the eclipse (Gies et al. 2002). The main criteria that the absorption lines are formed in the stellar photosphere are a "correct" behavior of their intensities and radial velocities with orbital phase.

Gies et al. (2002), Hillwig et al. (2004) detected weak absorption lines of TiII, FeII, CrII, SrII, CaI, FeI in the blue region 4100–4600 Å of the spectrum. They observed SS433 near the primary eclipse and in precession phases where the disk is the most "face-on". These lines are believed to belong to the donor star of SS433 with an A-type spectrum.

One may also try to search for stellar lines in yellow and red regions among the weakest metallic lines, however these regions are crowded with strong moving lines of hydrogen and HeI formed in the relativistic jets. The moving lines are extremely variable and have structured profiles. This complicates the searching for weak lines and studying their behavior from date to date. For this reason we have investigated only the bluer parts of our spectra. The most informative region for stellar line studies is 4200–4340 Å where no strong emission lines and no appreciable moving lines appear at these precession phases.

The 4100–5300 Å SS433 spectra have been compared with those of the known galactic supergiants with different temperatures. We used publicly available (http://webast.ast.obs-mip.fr/stelib/) library of stellar spectra (STELIB, Le Borgne et al. 2003). These spectra were taken with the same spectral resolution (3 Å) as our spectra of SS433. For identification of lines we have used spectral atlases of Deneb (A2 Iae) (Albayrak et al. 2003) and o Pegasi (A1 IV) (Gulliver et al. 2004). Spectra of SS433 summed over one night were used for the line identification.

7. Spectral type of the optical star

Fig. 15 shows spectra of four supergiants and two SS433 spectra taken outside and inside the eclipse, each averaged over two nights. The eclipse-out spectrum was averaged over nights 09.05.2003 and 12.05.2003 corresponding to evenly spaced from the eclipse center orbital phases 0.89 and 0.12 (the top spectrum). The eclipse-in spectrum was averaged over nights 28.04.2003 and 11.05.2003 corresponding to orbital phase 0.05 (second from the top spectrum in the figure). The supergiants shown in Fig. 15 are HD36673 (F0I, 7,200 K), HD39866 (A2I, 8,400 K), HD87737 (A0I, 9,700 K) and HD164353 (B5I, 22,000 K). All spectra were normalized and shifted along vertical axis for better visualization.

With our spectral resolution, practically all absorption lines appear as complex blends. In Fig. 15 the lines observed out of the eclipse are marked with short vertical bars; those which are seen in the eclipse or present in both spectra are marked with long bars. One can see that the strongest absorptions in the spectra of supergiants are also present in SS433 and these absorption lines are deeper in the spectrum during the primary

Table 4. Journal of spectral observations

Date	JD (mid) 2450000+	Orbital phase	Precession phase	N	Exposure (sec)	Range (Å)
28.04.2003	2758.491	0.054	0.973	8	900	4160–5400
09.05.2003	2769.466	0.893	0.041	3	600	5170–6410
09.05.2003	2769.507	0.896	0.041	4	900	3970–5220
10.05.2003	2770.458	0.969	0.047	4	600	5170–6410
10.05.2003	2770.501	0.972	0.047	4	900	3970–5220
11.05.2003	2771.490	0.048	0.053	8	900	4180–5430
12.05.2003	2772.508	0.126	0.060	4	900	4180–5430
13.05.2003	2773.492	0.201	0.066	4	900	4180–5430

minimum. FeIIλ4233 emission is seen (FWHM$\sim$ 10 Å), CIIλ4267 and NIIIλ4196, 4200 + HeIIλ4200 emissions are also marginally present.

The intensity of absorption lines during the eclipse allows us to estimate the effective temperature of the donor star to be $T < 9000$ K. This limitation was obtained from the fact that the absorption lines in SS433 can not be deeper than those in spectra of supergiants, because the accretion disk is not totally escipsed in the primary minima. The relative intensities of the strongest metallic absorption lines indicate a temperature of $T = 8000 \pm 500$ K, implying the optical spectral class of the companion A5-A7I.

7.1. Evidence for heating effect in the illuminated hemisphere

The analysis of different absorption lines of the optical star reveals a strong heating effect in the illuminated star's atmosphere. During the disk eclipse egress low-excitation absorption lines strongly weaken. The stellar hemisphere illuminated by the bright accretion disk in SS433 probably has a temperature of $\sim$ 20,000 K, as the presence of CIIλ4267 absorption + emission line suggests (the top spectrum in Fig. 15). This absorption line is the strongest one in this spectral region among supergiants with temperatures T> 15,000 K. The evolution of the blend λ4273 (FeIλ4271.7 + FeIIλ4273.3 + CrIIλ4275.5) is seen: in the eclipse center the low-excitation line FeI is stronger, while out of the eclipse FeII+CrII lines enhance. Other FeI lines also appear only in the eclipse.

These effects are illustrated by Fig. 16, in which spectra of the standard stars with effective temperatures 8,400 K and 22,000 K are shown together with spectra of SS433 obtained in 9.05, 10.05, 28.04+11.05, 12.05 and 13.05 (orbital eclipses fell in nights 10.05 and 28.04+11.05). The orbital phase rises from bottom to top in the figure. There are emission lines in these spectral fragments — the broad structured emission of CIIλ4267, and stronger emissions FeIIλ5169+MgIλ5167, 5173 and FeIIλ5197. Note that emission lines, which are formed presumably in the disk wind, should move blueward (in phase with the compact object) in the orbital phases of our observations. In contrast, absorption lines, which are formed in the donor photosphere, must move redward during our observations. A strength of the CIIλ4267 absorption component (marked by vertical bars in Fig. 16) increases notably out of the eclipse. The complex blend λ4273 (FeI+FeII+CrII) is marked by the dotted lines in the figure.

Fig. 16 illustrates absorption lines (marked by the vertical bars) — the blend λ4314 of TiIIλ4313+FeIIλ4314+TiIIλ4315; ScIIλ4320 line and the blend ScIIλ4325 + FeIλ4326, 4327. However the last blend may be distorted by the strong blue wing of Hγ in the middle of eclipse. Other absorption lines shown in Fig. 16 (right panel) are λ5154 (TiII+FeII) and λ5227 (TiII+FeI). It is seen that these lines shift redward with time.

In Fig. 16 we also show a spectrum of SS433 averaged over all nights of observations (the third from bottom spectrum). When averaging spectra obtained in individual nights we shifted them to zero velocity according to the radial velocity curve from Fig. 18. The average spectrum has a better signal-to-noise ratio. All the absorpton lines remain in the spectrum and they are similar to the corresponding lines in the spectrum of the standard supergiant (8,400 K). The shallow emission line (presumably CIIλ4267) has an absorption component. In our recent spectral observations of SS433, which were carried out around primary mimima on August 24, 2004 and September 6, 2004 (the precession phase is the same, i.e. the maximum disk opening) we confirmed the presence of the absorption lines studied in this paper. Both the spectral resolution and signal-to-noise ratio are better in the new observations. Analysis of the new data will be published elsewhere.

7.2. Measurements of the radial velocity of the optical star

It is important to stress that the strongest absorptions (FeII, HeI) are disfavored for the optical star radial velocity analysis, as they most probably formed in the powerful outflowing disk wind (Fabrika et al. 1997). We studied radial velocities of weak absorption lines of metals. It is easy to confuse the line identification when one traces a line from date to date because of the spectral variability and orbital motion of the companions. In Fig. 17 we present individual absorption line radial velocities for four best-

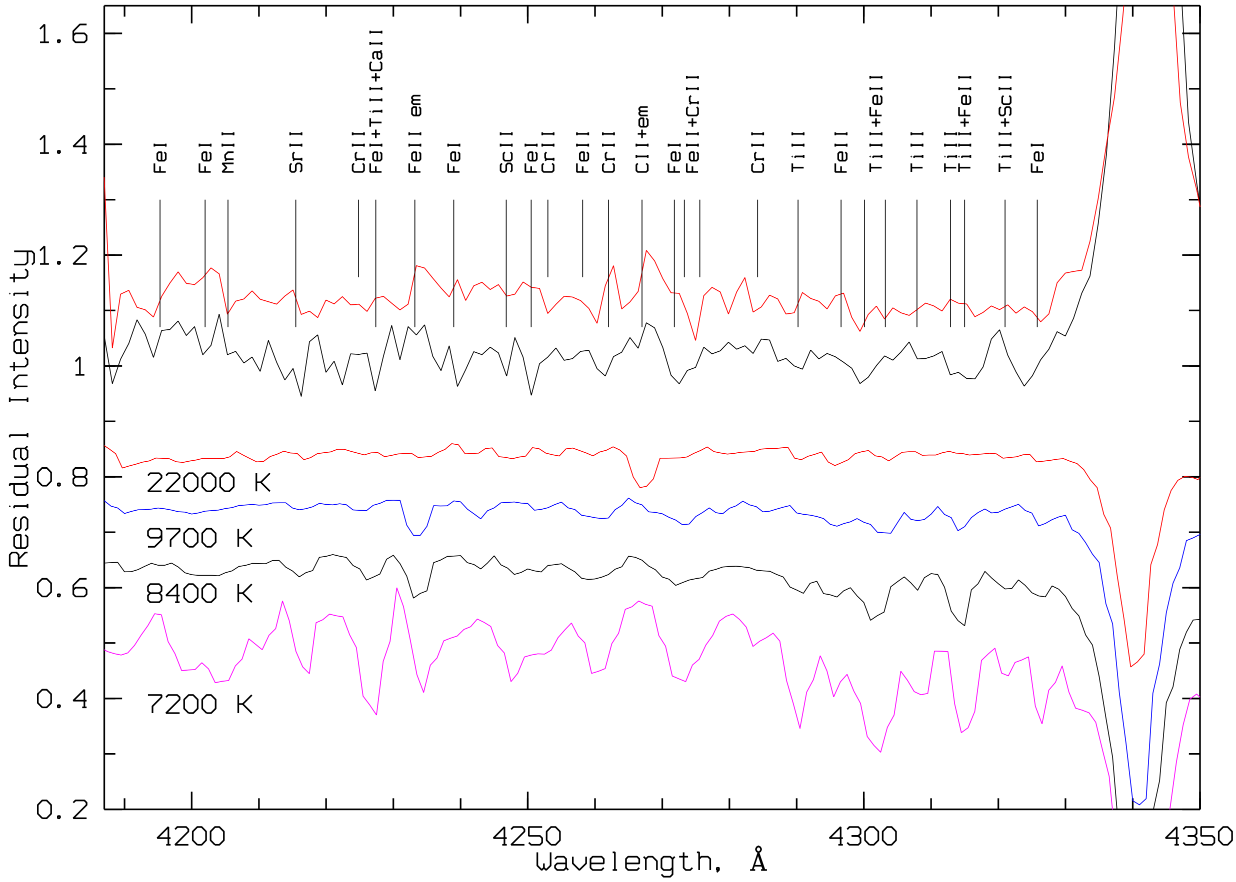

Fig. 15. Spectra of SS433 and spectra of four supergiants of known temperatures (Le Borgne et al., 2003) for a comparison. The top spectrum was taken outside the eclipse and averaged over nights 09.05.2003 and 12.05.2003 (evenly spaced from the eclipse center orbital phases 0.89 and 0.12). The second from the top spectrum was taken inside the eclipse and averaged over nights 28.04.2003 and 11.05.2003 (the orbital phase 0.05).

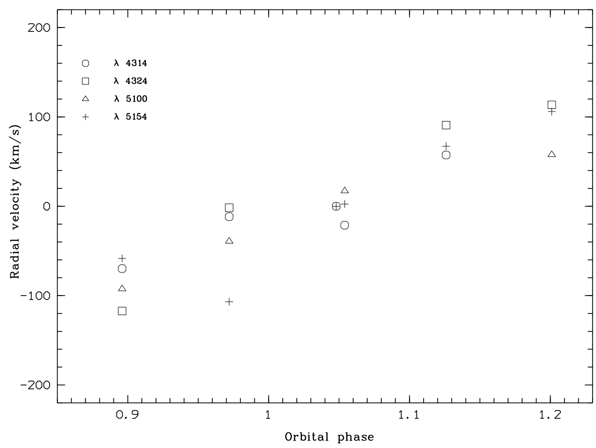

Fig. 17. Radial velocity curve of the optical companion of SS433 obtained from 4 individual absorption lines over 6 nights.

suited lines averaged over one night, as a function of the orbital phase for 6 nights.

The radial velocity curve measured by the most reliable collection of 22 absorption lines in the spectral range 4200-5300 Å is shown in Fig. 18. Note that with our spectral resolution the absorption lines in the SS433 spectrum are seen as blends containing 2-3 lines, and we measured their relative radial velocities because of unknown "laboratory" wavelengths of the blends. Relative intensities of the lines change from date to date through the eclipse. For this reason we measured only those lines and in only those dates where the lines were the most convincingly detected. The radial velocity curve (Fig. 18) has been obtained by coadding radial velocity curves of individual lines, and the zero radial velocity of all lines in 11.05.2003 (the orbital phase 0.048) was adopted. If a line was not detected in 11.05.2003, the zero radial velocity was assumed for 28.04.2003 as well (the orbital phase 0.054). If the measured radial velocity in 11.05.2003 disagreed with the whole radial velocity curve of a given line, an additional shift for the curve was applied. However no shifts in excess of 20 km/s were done. This is the reason why the radial velocity error in 11.05.2003 is small, but not zero.

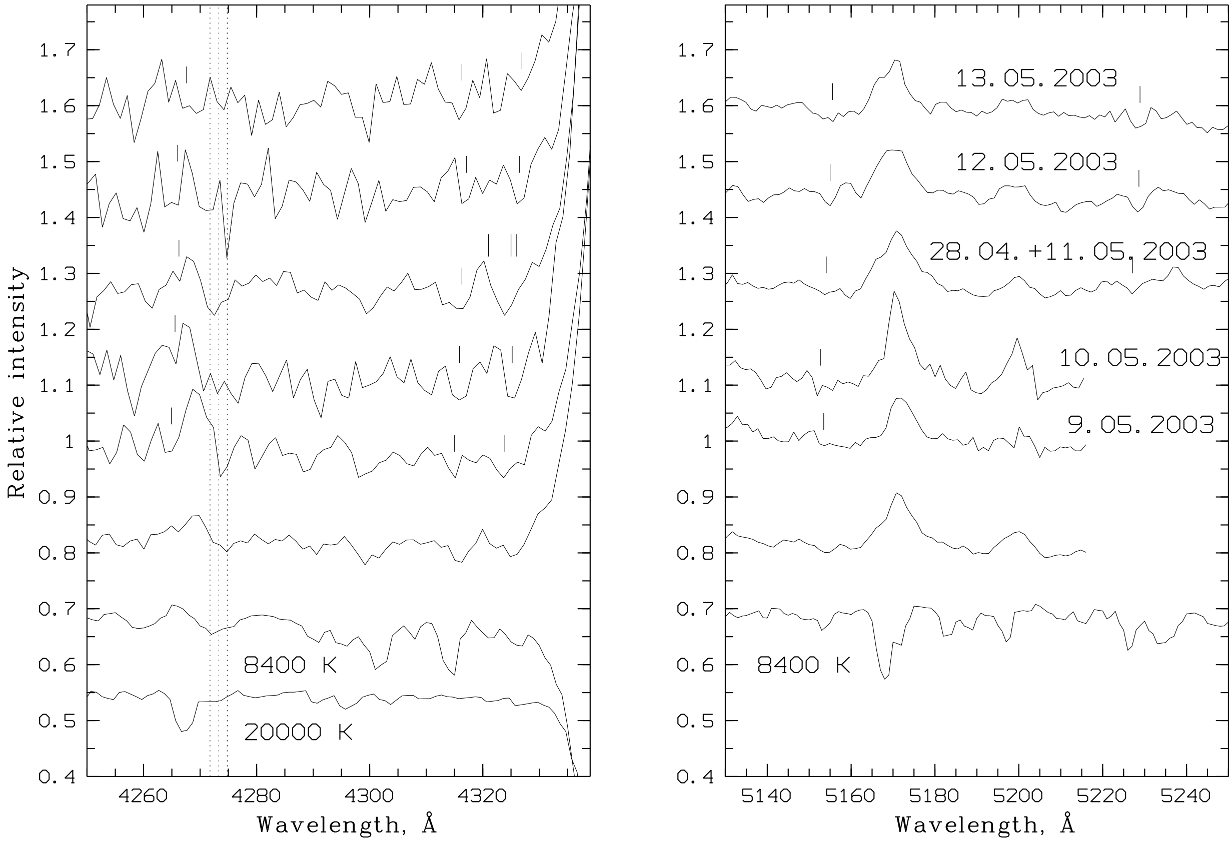

Fig. 16. Evolution of absorption lines in the optical spectra of SS433 taken at different orbital phases (see Table 4). For comparison, spectra of two supergiants (8,400 K and 22,000 K) are shown in the bottom. Radial velocity of the optical star is traced by different absorption lines (vertical bars). On the left panel, the third from bottom is the SS433 spectrum averaged over all nights with taking into account the radial velocity shifts from Fig. 18. See the text for more detail.

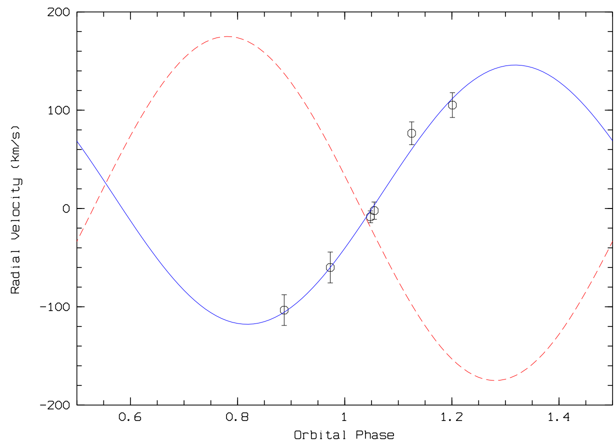

Fig. 18. Mean radial velocity curve of the optical companion of SS433 measured from 22 individual absorption lines. The accretion disk radial velocities as measured by HeIIλ4686 emission (Fabrika and Bychkova, 1990) is shown by the dotted line.

So the radial velocity curve for absorption lines in Fig. 18 consists of individual radial velocity curves. Each point of the curve includes from 10 to 17 individual measurements. Most measurements were carried out at the primary minimum as there the absorption lines are deeper.

The derived radial velocity semi-amplitude of the donor star is $K_v = 132 \pm 9$ km/s, the gamma-velocity of the binary system is $v_\gamma = 14$ **km/s with formal fit uncertainty** 2 **km/s.** The absorption line radial velocity transition through the γ-velocity occurs at the middle of the optical eclipse ($\phi_b = 0.07$), confirming that the lines actually belong to the donor star. Note that in the gamma-velocity v_γ and in the transition phase ϕ_b some systematic errors can be present because of the method used. However they are less than 30 km/s (no bigger shifts were applied to radial velocity curves of individual lines) and 0.05 correspondingly. The main observational bias in studying radial velocities of the donor star is the faintness of absorption lines outside the primary minima and strong intrinsic spectral variability of SS433. To confirm the derived radial velocity curve further spectral observations are needed.

Our results confirm the earlier determination of K_v by Gies et al. (2002) which were carried out also at the maximum disk opening phases. Note that spectroscopic observations by Charles et al. (2004) were performed at the crossover phase of SS433 when the accretion disk is

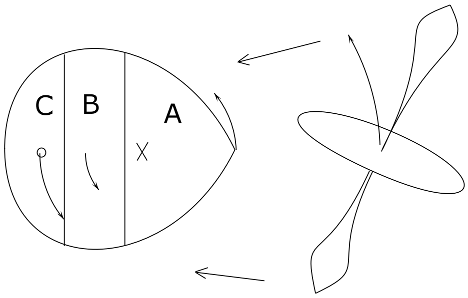

Fig. 19. The spectroscopic center of the normal star (circle) heated by its companion is shifted with respect to the gravity center (cross). The arc arrows indicate the orbital motion. Zone "A" is the most effectively illuminated by the compact source, disk and jet. Zone "B" is also illuminated by outer parts of disk and jet and by scattered radiation. The low excitation potential absorption lines used for radial velocity measurements can be formed in zone "C" which is not heated. Due to this effect, the spectroscopically derived radial velocity of the optical star is overestimated.

seen edge-on. Such a phase is disfavored for the donor star radial velocity analysis as strong gas outflows contaminate the disk plane; selective absorption in this gas affects the true radial velocity of the donor star.

The heating effect of the donor star also distorts the radial velocity semi-amplitude. The analysis (Wade and Horne 1988, Antokhina et al. 2005) indicates that the true value of the semi-amplitude of the radial velocity curve as derived from these absorption lines can be reduced to ~ 85 km/s (see below).

Recently Hillwig et al. (2004) obtained an estimate of the radial velocity amplitude of the donor star $K_v = 45 \pm 6$ km/s and the gamma-velocity $v_\gamma = 65 \pm 3$ km/s. In our opinion, some strong lines (which actually are shell-like lines on the background of faint emission) could contribute to the radial velocity cross-correlations of Hillwig et al. (2004). For example, the two strongest lines in their Fig. 5 FeIIλ4550 and FeIIλ4584 are in emission in our spectra in the middle of eclipse.

The KPNO-2003 observations of Hillwig et al. (2004) were in the orbital phases 0.85-1.07. Absorption lines formed in rotating and extended envelope of the donor could be probably observed. In these orbital phases, the side of the envelope projected onto the strong continuum source (the accretion disk) moves away from the observer. Then the amplitude of the line shift can be expected to be $\sim 1/2 V_{equat} \sim 60$ km/s. This might explain the positive shift of the system's velocity +65 km/s found by those authors.

8. Implications to binary masses

Comparison of radial velocities of the accretion disk ($K_x = 175$ km/s, Fabrika and Bychkova 1990) and optical star ($K_v = 132$ km/s) yields the mass ratio in the SS433 system $q = m_x/m_v = K_v/K_x = 0.75$ (here m_x and m_v stand for relativistic object and optical star mass, respectively). Taken at face value, these q, K_v would lead to the optical star mass function $f_v \approx 3.12 M_\odot$ and the binary component masses $m_x = 18 M_\odot$, $m_v = 24 M_\odot$. However, such a big mass ratio is in a strong disagreement with the observed duration of X-ray eclipse, which suggests much smaller mass ratio $q \sim 0.2-0.3$. We stress that the binary inclination angle in SS433 ($i = 78^o.8$) is fixed from the analysis of moving emission lines.

There are two possibilities: (1) either the model we used to fit X-ray eclipses should be modified, or (2) the value of K_x and K_v are influenced by additional physical effects. Though there are some reasons to modify the model (e.g., the asymmetric shape of the hard X-ray eclipse, which may suggest an asymmetric wind outflow from the illuminated part of the optical star and wind-wind collision), we shall consider here only the second possibility. The reason is that the actual value of K_v should be decreased in order to account for the observed heating effect.

Let us assume the mass ratio in the system to be $q = 0.3$, as with this value we can satisfactorily describe the width of X-ray eclipse and the observed X-ray precession amplitude (see Fig. 10). Taking $K_v = 132$ km/s yields $f_v \approx 3.1 M_\odot$ and $m_x = 62 M_\odot$, $m_v = 206 M_\odot$, $K_x = 440$ km/s. Clearly, this is an unacceptable model. Now let us decrease K_v down to 85 km/s, the lower limit which follows from a more accurate treatment of the heating effect in the radial velocity curve analysis (Wade and Horne 1988, Antokhina et al. 2005). This would yield a better fit with $m_x = 17 M_\odot$, $m_v = 55 M_\odot$, and $K_x = 283$ km/s, still too high to be acceptable. Finally, let us take into account that less than half of the stellar surface is sufficiently cool to give the absorption lines under study (e.g. due to sideway heating from scattered UV radiation in the strong accretion disk wind). This additionally decreases the value of the actual radial velocity semi-amplitude. Fig. 19 illustrates these considerations.

So taking, for example, $K_v = 70$ km/s and $q = 0.3$ yields the optical star mass function $f_v = 0.46 M_\odot$, binary masses $m_x = 9 M_\odot$, $m_v = 30 M_\odot$ and the optical star radius $R_v \sim 40 R_\odot$. This radius is compatible with typical bolometric luminosity of a $30 M_\odot$ A5-A7 supergiant with $T_{eff} \sim 8500$ K. In this solution, $K_x \simeq 233$ km/s, larger than the measured value 175 km/s, but the true value of K_x may be affected by the strong accretion disk wind.

9. Discussion

The interpretation of the binary parameters presented above is strongly based on the binary mass ratio $q = 0.3$ as inferred from modeling the *INTEGRAL* observations of the hard X-ray eclipse with account of the observed amplitude (~ 4) of the hard X-ray precessional variability of the system. The model we use (optical star filling its Roche lobe + thick accretion disk with a hot corona) is simplistic and cannot reproduce perfectly the apparent asymmetric shape of the X-ray eclipse. In real situation, an additional

X-ray absorption by outflowing gaseous streams, extended stellar envelope or wind seems quite plausible. If we interpret the complex shape of the hard X-ray egress as being due to additional variable absorption effects, we obtain the geometry of the hard X-ray emitting region in the form of an extended oblate corona over the accretion disk. However, a straightforward interpretation of the joint RXTE+*INTEGRAL* spectrum of the source observed in March 2004 is also possible by a single thermal emission with a temperature of $\sim$ 30 keV. No additional emitting region is required to fit this broadband X-ray spectrum.

There are two possible ways out of this. First, we could try to describe the observed hard X-ray spectrum by a more complex model involving two components, a hot corona + cooler thin jet radiating in the standard X-ray band. Second, we could try to accept the thin cooling jet interpretation of the X-ray spectrum, but then would have to admit a different actual shape of the X-ray eclipse. Our modeling shows that a thin short jet could reproduce the observed amplitude (~ 4) of hard X-ray precessional variability in SS433. In that case, the shape of the X-ray eclipse must be more sharp, with shorter ingress/egress time than actually observed (cf. Fig. 9). If we look at the data, such a shape can indeed be found at the egress phase of the eclipse (see Fig. 6). The (apparently longer) ingress time could be due to additional (apart from the opaque star body) absorption of hard X-ray emission by optically thick gaseous stream outflowing from the optical star. Apparently the same smooth ingress and egress shape of the eclipse in softer X-rays (the *Ginga* and *ASCA* data) could be in that case due to the soft X-ray emitting region locating further upstream the jets. This interpretation also explains more shallow soft X-ray eclipse.

Clearly, in this situation we need more observations of the hard X-ray eclipse to confirm the asymmetric ingress/egress eclipse shape and flatness of its bottom. We hope to do this in future *INTEGRAL* observations of SS433.

10. Conclusions

The results of the *INTEGRAL* observations of the peculiar binary system SS433 in 2003-2004 can be summarized as follows.

1. Hard X-ray emission up to $\sim$ 100 keV is discovered from this superaccreting microquasar with uneclipsed hard X-ray luminosity close to the maximum opening precession phase $L_x(18-60\text{keV}) \sim 4\times10^{35}$ erg/s, $L_x(60-120\text{keV}) \sim 2\times10^{35}$ erg/s (assuming the 5 kpc distance to SS433), which is about 10% of the soft X-ray jet luminosity.

2. Persistent precessional variability in hard X-rays is discovered with the maximum to minimum flux ratio ~ 4, which is twice as large as in softer X-ray band.

3. The observed hard X-ray orbital eclipse is found to be in phase with the optical and near infrared eclipses. The hard X-ray eclipse is observed to be at least two times deeper than soft X-ray eclipse. The width of the X-ray eclipse increases with energy, which is opposite to what is observed in classical X-ray binary systems.

4. The broadband X-ray spectrum 2-100 keV of SS433 simultaneously obtained by *INTEGRAL* and RXTE in March 2004 when the source was in its flaring state can be fitted by bremsstrahlung emission from optically thin plasma with temperature $kT \approx 30$ keV.

5. Optical spectroscopic observations of SS433 on the SAO 6-m telescope which were performed in the framework of the multiwavelength *INTEGRAL* campaign of the source confirmed the spectral class of the optical star to be A5-A7I. The radial velocity curve of the optical component is obtained with semi-amplitude $K_v = 132 \pm 9$ km/s near the maximum disk opening precession phase (T3). The spectroscopic data discovered the heating effect of the hemisphere of the optical star illuminated by the accretion disk.

6. From the analysis of the hard X-ray eclipse and precession variability in SS433 we estimate the mass ratio in this binary system to be $q \sim 0.3$. This mass ratio and radial velocity measurements corrected for the heating effect enable us to evaluate the masses of the optical and compact star in SS433 to be $M_v \approx 30 M_\odot$, $M_x \approx 9 M_\odot$, **respectively**. This finding lends further support to the presence of a black hole in this peculiar superaccreting galactic microquasar.

Acknowledgements. The authors thank E.M.Churazov for developing methods and analysis of the IBIS data and software. We acknowledge Vitaly Goranskij for comments and discussion. We also ackhowledge E.K. Sheffer, S.A. Trushkin, V.M. Lyuty, S.Yu. Shugarov, N.A. Katysheva, A.A. Lutovinov for discussions and collaboration. We especially thank Dr. D. Hannikainen for providing us with data on SS433 X-ray egress observations and M.G. Revnivtsev for processing *RXTE* spectra of SS433. IFB thanks the Turkish National Observatory night assistants Kadir Uluc and Murat Parmaksizoglu for their support in the photometric SS433 observations. A.N. Burenkov is acknowledged for a help in spectral observations. The work of SNF is partially supported by the RFBR grant 04-02-16349. The work of KAP, ANT and IEP is partially supported by the RFBR grant 04-02-16720. The work of KAP was also partially supported by the Academy of Finland through grant 100488. NIS and IEP acknowledge the financial support from the RFBR by the grant 03-02-16068. SVM and ES acknowledge the European Space Agency for support and the Integral Science Data Center (Versoix, Switzerland) for providing computing facilities. ANT also acknowledges the financial support from the Russian Federation President Grant Program through grant MK-895.2003.02. The work of AMCh, EAA, EVS and ANT was partially supported through the grant of Leading Scientific Schools of Russia NSh-388.2003.2 and RFBR grant 02-02-17524. NAS and IFB acknowledge the support of RFBR grant 02-02-17174 and grant of Leading Scientific Schools of Russia NSh-1789.2003.2. EAB was partially supported by the RFBR grant 03-02-16133. The IR observations (YNG and AAA) are partially supported by the RFBR grant 03-02-17223a , the Program of Prezidium RAN "Nonstationary Processes in Astronomy" and the FBNTP "Astronomy". We are grateful to the anonymous referee for the useful remarks which helped us to improve and clarify the article.

References

Afanasiev V.L., Burenkov A.N., Vlasyuk V.V., Drabek S.V., 1995, SAO RAS internal report No.247

Albayrak, B. Gulliver, A.F., Adelman, S.J., Aydin, C., Kocer, D. 2003, A&A, 400, 1043

Antokhina E.A., Seifina E.V, Cherepashchuk A.M., 1992, SvA 36, 143

Antokhina E.A., Cherepashchuk A.M., Shimansky V.V., 2005, Astron. Rep., v.49, N1, in press

Aslanov A.A., Cherepashchuk A.M., Goranskij V.P., Rakhimov V.Yu., Vermeulen R.C., 1993, Astron. Astrophys. 270, 200

Begelman, M.C., Blandford, R.D. and Rees, M.J. 1984, Rev. Mod. Phys. 56, N 2, 1

Chakrabarti, S. K. In "Exotic Stars as Challenges to Evolution", ASP Conference Proceedings, Vol. 279. Also IAU Colloquium 187. Edited by Christopher A. Tout and Walter Van Hamme. San Francisco: Astronomical Society of the Pacific, 2002., p.5

Charles P.A., Barnes A.D., Casares J., et al., 2004, *astro-ph/0402070*

Cherepashchuk A.M., 1988, Sov. Sci. Rev. Ap. Space Phys., Ed. by R.A.Sunyaev, v.7, p.1

Cherepaschuk, A. 2002, Space Sci. Rev. 102, 23

Cherepashchuk A.M., Yarikov S.F., 1991, *SvA Let.* 17, 258

Cherepashchuk A.M., Sunyaev R.A., Seifina E.V., et al., 2003, Astron. Astrophys. 411, L441

Cherepashchuk A.M., Sunyaev R.A., Fabrika S.N., et al., 2004, in Proc. V INTEGRAL Workshop, ESA SP-552, in press (astro-ph/0404479)

Clark D.H., Murdin P., 1978, Nature 276, 54

Crampton, D., Hutchings, J.B. 1981, Vistas Astron. 25, 13

Fabrika S.N., 2004, Astrophys. Space Phys. Rev. 12, 1

Fabrika S.N., Bychkova L.V., 1990, *AA* 240, L5

Fabrika S.N., Bychkova L.V., Panferov A.A., 1997, Bull. Spec. Astrophys. Obs. 43, 75

Fabrika S.N., Abolmasov P., Irsmambetova T., 2004, in preparation

Fabrika S., Irsmambetova T., 2002; In *'New Views on Microquasars"*, the Fourth Microquasars Workshop, Ph. Durouchoux, Y. Fuchs, J. Rodriguez (eds). Center for Space Physics, Kolkata (India), p.268

Gies D.R., Huang W., McSwain M.V., 2002, ApJ 578, L67

Gladyshev S.A., Goranskii V.P., Kurochkin N.E., and Cherepashchuk A.M., 1980 Astron.Tsirk. No 1145, p.1

Goranskij V.P., Esipov V.F., Cherepashchuk A.M., 1998a, Astron. Rep. 42, 209

Goranskij V.P., Esipov V.F., Cherepashchuk A.M., 1998b, Astron. Rep. 42, 336

Gulliver, A.F. Adelman, S.J., Friesen, T.P. 2004, Astron. Astrophys, 413, 285

Hillwig, T.C., Gies, D.R., Huang, W., McSwain, M.V., Stark, M.A., van der Meer, A., Kaper, L. 2004, astro-ph/0403634

Kawai N., Matsuoka M., Pan H.-C., Stewart G.S., 1989, PASJ 41, 491

Kotani T., Kawai N., Matsuoka M., Brinkmann W., 1996, PASJ 48, 619

Le Borgne J-F., Bruzual G., Pello R., et al., 2003, Astron. Astrophys. 402, L433

Leibowits E.M., Mendelson H., 1982, *PASP* 94, 977

Lind, K.R. and Blandford, R.D. 1985, ApJ 295, 358

Margon B., 1984, ARAA 22, 507

Margon B., Ford H.C., Katz J.I. et al., ApJ 230, L41

Panferov, A.A. and Fabrika, S.N. 1997, Astron. Rep. 41, 506

Revnivtsev M.G., Burenin R., Fabrika S.N., et al., 2004a, Astron. Astrophys. in press (astro-ph/0405388)

Revnivtsev M.G., Sunyaev R.A., Varshalovich D.A., et al., 2004b, Astron. Lett. in press (astro-ph/040202)

Shakura N.I., Sunyaev R.A., 1973, Astron. Astrophys. 24, 337

Trushkin, S.A., Bursov, N.N. and Smirnova, Yu.V. 2001, Astron. Rep. 45, 804

Trushkin S.A., 2003, *Bull. Spec. Astrophys. Obs.* 56, 57 (astro-ph/0403037)

Trushkin, S.A. 2004, http://cats.sao.ru∼satr/XB/SS433/

Wade R.A., Horne K., 1988, ApJ 324, 411

Yuan W., Kawai N., Brinkmann W., Matsuoka M., 1995, Astron. Astrophys. 279, 451

Zwitter N., Calvani M, D'Odorico. S, 1991, Astron. Astrophys. 251, 92